Geotechnical Aspects of Underground Construction in Soft Ground – Viggiani (ed)
© 2012 Taylor & Francis Group, London, ISBN 978-0-415-68367-8

Experimental and numerical study of grout injections in silty soils

L. Masini & S. Rampello
"Sapienza", University of Rome, Italy

G.M.B. Viggiani
"Tor vergata", University of Rome, Italy

K. Soga
University of Cambridge, Cambridge, UK

ABSTRACT: Compensation grouting is increasingly employed as a mitigation technique of settlements induced by tunnelling and its effectiveness both in clayey and sandy soils is reported in a wide number of case histories. However, the results are highly dependent on grout properties, injection characteristics and soil properties. An experimental study was conducted to investigate the parameters that control grout injections in silty soils. The results from one injection test in a large sample of silty soil show that the compensation efficiency, defined as the ratio of the volume of heave obtained at ground surface and the injected grout volume, is much lower than one and tends to decrease with time, while the initial volume of grout lost due to pressure filtration is small. Finally, results from finite elements back analyses of the laboratory test show that a good agreement with the experimental data can be obtained if the development of large strains is taken into account.

1 INTRODUCTION

Compensation grouting has become a widely used technique to protect existing structures from excessive settlement induced by tunnelling carried out in densely built urban areas. Figure 1 shows a scheme of application of compensation grouting to compensate for tunnelling induced settlements. Basically, grout is injected in the zone between the tunnel crown and the foundations of the structure to compensate for the stress relief due to the excavation process (Mair & Hight 1994). The injection is carried out through sleeved tubes (*tubes à manchette*) which can be installed from a vertical shaft in a fan shaped array.

The effectiveness of compensation grouting can be quantified using the compensation efficiency ξ, defined as the ratio of the volume of heave obtained at ground surface, V_{SH}, and the injected grout volume, V_{inj} (Au *et al*. 2002):

$$\xi = V_{SH}/V_{inj}$$

Ideally, if soil deformation due to the injection process occurred in undrained conditions, ξ would be equal to one, as the volume of injected grout would produce the same amount of heave at ground surface. In practice V_{SH} is always less than V_{inj} ($\xi < 1$) because of volume loss due to several reason. In normally consolidated clayey soils it has been shown (Au 2001, Au *et al*. 2003) that ξ decreases with time due to soil consolidation, as positive excess pore water pressure is induced during the injection process. Long term efficiency could even reach negative values, *i.e.* grout injections could produce long term settlements rather than heave.

In sandy soils, the experimental findings (McKinley 1993, McKinley & Bolton 1999, Sanders 2007, Bezuijen *et al*. 2007, Eisa 2008) show that the injection pressure causes a mixture of water and finer particle to filtrate from the grout body into the adjacent sand pores. Compensation efficiency reduces as pressure filtration occurs. The amount of fluid lost by pressure filtration depends on the grout water-cement ratio and bentonite content, and on the injection rate. Eisa (2008) has shown that fast injections of grout with relatively high bentonite content and water-cement ratio result in low volumes lost by pressure filtration and high compensation efficiencies.

This study focuses on grout injections in silty soils. To this aim, laboratory grout injections tests

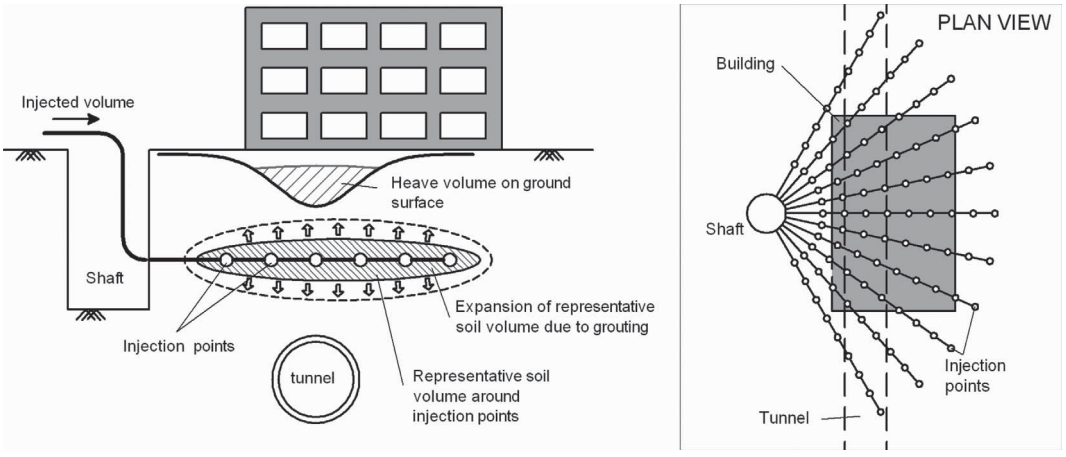

Figure 1. Schematic field layout of grout injection to compensate for tunneling induced settlement.

were preformed in a large sample of normally consolidated silty soil. The injection pressure, the sample surface displacements, the volume of fluid drained from the sample, and the stresses and pore water pressures at different locations in the sample were measured during and after the tests. In the following, the results of the tests are first illustrated and then compared to the experimental findings obtained for grout injections in clayey and sandy soils.

Finite-element analyses were also conducted to simulate the grout injection test. The results of these analyses are compared with the experimental data in terms of ground surface displacement, excess pore water pressure and stress changes. The analyses were carried out assuming large strains.

2 EXPERIMENTAL WORK

2.1 *Testing apparatus and methods*

The laboratory investigation was conducted at the Schofield Centre of the University of Cambridge (UK). The experimental setup used for the grout injection test is shown in Figure 2. A cylindrical steel tub with an internal diameter of 850 mm and a height of 400 mm is used to contain the sample. Drainage of fluid from the sample is allowed from the base of the tub through a drainage layer, consisting of sand, gravel, geotextile, and filter paper. A confining pressure is applied to the top of the sample by inflating with pressurised air a rubber bag fixed to the inner side of the tub cover. An open-ended metallic tube (inner diameter 7.5 mm, external diameter 12.5 mm) was used to inject the

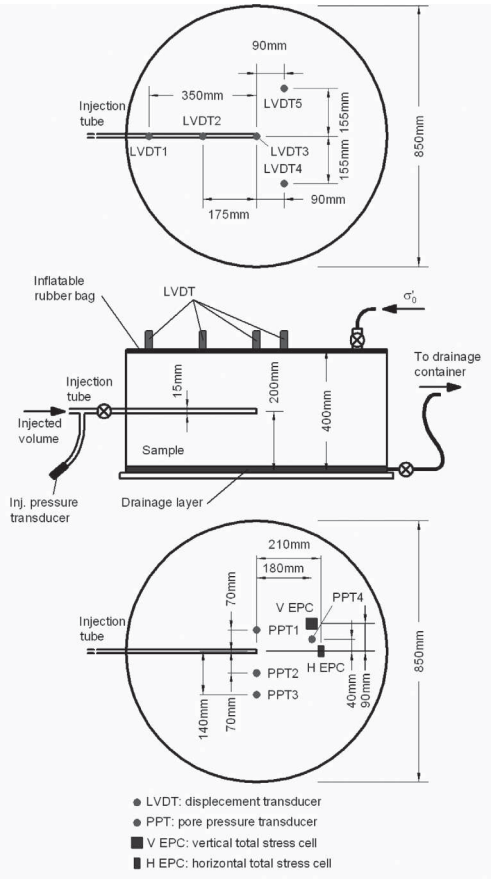

Figure 2. Experimental setup and instruments location.

grout. The injection point is located approximately at the centre of the sample. Grout is injected using a progressive helical cavity pump. Five displacement transducers (LVDTs), located in the positions shown in Figure 2, are used to measure the displacements at the sample surface during and after the injection. The spindle of each LVDT passes through a hole in the cover of the tub and rests on a thin latex membrane sealed on the sample surface to prevent water from leaking out. The rubber bag used to apply the confining pressure is sealed around the five LVDTs spindle holes. Two earth pressure transducers (EPCs) for the horizontal and vertical total stress and four pore water pressure transducers (PPTs) are installed inside the tub at the level of the injection point and at different distances from it. A pressure transducer (PT) installed along the injection tube, just outside the tub, measures the injection pressure.

The grout injection test was performed in a large sample of silica flour.

Table 1 lists the physical properties of type 3045/300 silica flour ($D_{10} = 7\,\mu m$, $D_{50} = 16\,\mu m$) which was used in the experiment (Silva 2005). The sample was prepared from a slurry with a water content of 58%, or twice the liquid limit. The slurry was poured into the tub and vibrated, and then allowed to sediment under its own weight overnight. Finally, the slurry was consolidated to the confining pressure chosen for the test (100 kPa in this case). After the test, measurements of void ratio made on the soil extracted from two boreholes located away from the injection body showed a good homogeneity of the sample, with an average void ratio of 0.83.

Grout is a mixture of water, cement and bentonite. Before the test, the bentonite was allowed to hydrate for 24 hours, and then mixed with cement using a high shear mixer. A total volume of 1000 cm^3 of grout was injected at a constant rate of 47.8 cm^3/s under a confining pressure σ_{conf} = 100 kPa, applied at the top of the sample. A relatively fluid grout was injected (water cement ratio $a/c = 1.8$), with a bentonite content equal to 8% of the weight of water.

For ease of reference, Table 2 summarises all the main parameters of the test; further experimental details can be found in (Au 2009 and Masini 2010).

Table 1. Physical properties of silica flour (Silva 2005).

Specific gravity of soil particles	G_S	2.652
Liquid limit	w_L	29%
Plastic limit	w_P	27%
Plasticity index	I_P	2%
Minimum void ratio	e_{min}	0.72
Maximum void ratio	e_{max}	1.83

Table 2. Parameters of the injection test.

Sample void ratio	e_0	0.83
Confining pressure	σ_{conf}	100 kPa
Injection rate	v_{inj}	47.8 cm^3/s
Injected volume	V_{inj}	1000 cm^3
Grout water-cement ratio	a/c	1.8
Grout bentonite-water ratio	b/a	8%

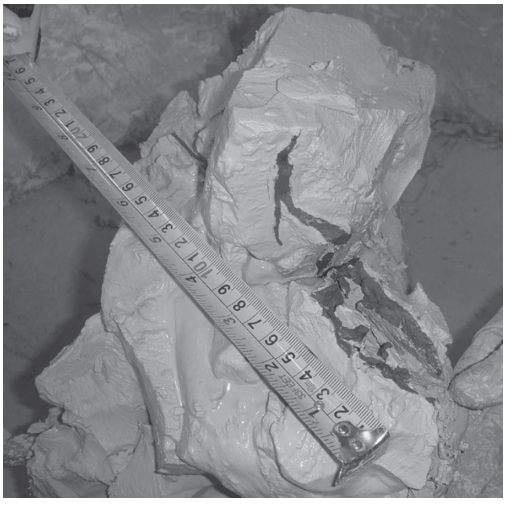

Figure 3. Grout injection in silt.

2.2 *Results*

Figure 3 shows the exhumed injection body 24 h after the test; a narrow fracture was observed to develop almost vertically from the injection point. Propagation of grout within the soil is influenced by the stress state in the soil. In fact, it has been found that fracture orientation is parallel to the major principal stress, in this case the vertical one (Jaworski *et al*. 1981, Mori & Tamura 1987, Mhach 1991, Murdoch 1993, Yanagisawa & Ali 1994).

Previous experimental findings (Sanders 2007, Eisa 2008) show that high viscosity grouts propagate close and uniformly around the injection point, while low viscosity grouts result in soil fracturing. Since grout viscosity increases with the volume of grout fluid lost by pressure filtration, the way grout propagates within soil is affected by pressure filtration. This feature can hardly be applied to clayey soil, as their low permeability permits only a very slow filtration to take place from the injection body.

Figure 4 shows the grout body from a test carried out using the same experimental setup, with the same grout and injection parameters listed in Table 2, but in dense sand (Eisa 2008, Masini 2010). In dense sand (relative density of 90%),

Figure 4. Grout injection in sand (Gafar 2008, Masini 2010).

grout viscosity increased significantly during the injection process because of pressure filtration, causing thick fractures into the soil. Conversely, in silty soil, the volume of grout fluid lost by pressure filtration during the injection process was negligible (see Figure 5) and grout viscosity was low enough to create narrow fractures. Similar findings have been obtained in clayey soils (Au 2001).

Figure 6 shows the displacement contours and profiles at the top of the sample measured at the end of the injection process. Positive displacements indicate heave. The compensation efficiency ξ was estimated from the ratio of heave to injected volumes.

The maximum heave ($w = 2.36$ mm) was obtained above the injection points. Major displacements were also observed along the injection tube due to some grout propagation just underneath the injection tube. This zone, indeed, is the most affected by the presence of the injection tube during sample preparation. This aspect together with the development of vertical fractures and the possible presence of some air bubbles in the system, resulted in low compensation efficiency ($\xi = 26\%$).

Figure 7 shows time variation of compensation efficiency ξ and the results obtained by Au (2001) injecting different fluids (grout with different water-cement ratio, epoxy resin and water) in normally consolidated (OCR = 1) samples of kaolin. Compensation efficiency decreases with time due to dissipation of the positive excess pore water pressure induced during injection, as shown in Figure 8. The long-term efficiency in silt ($\xi = 13\%$, $t = 12000$ s) was half the value at the end of injection process ($\xi = 26\%$), whereas large negative long-term values of ξ were obtained in clay, meaning that injections eventually caused settlement rather than heave. Therefore, even if compensation efficiency sensibly

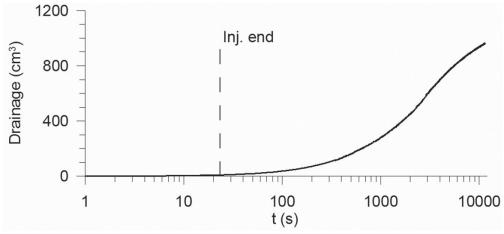

Figure 5. Volume of fluid drained from the sample.

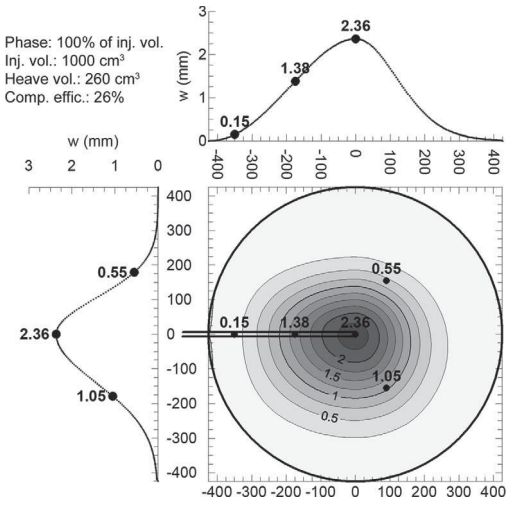

Figure 6. Displacement isolines (mm) and profiles at the top of the sample, obtained at the end of the injection process.

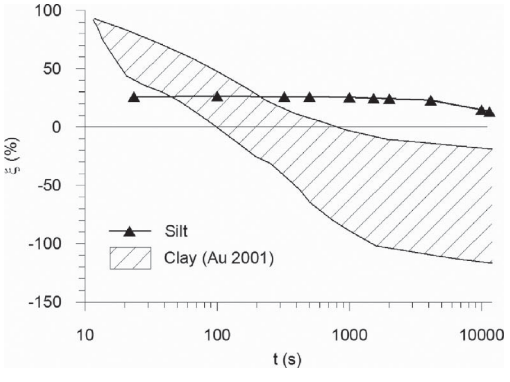

Figure 7. Time variation of compensation efficiency in normally consolidated (OCR = 1) samples of silt and clay (Au 2001).

decreases with time because of consolidation, it can be thought that long-term efficiency in normally consolidated silty soils is still positive, unlike what is observed for clayey soils.

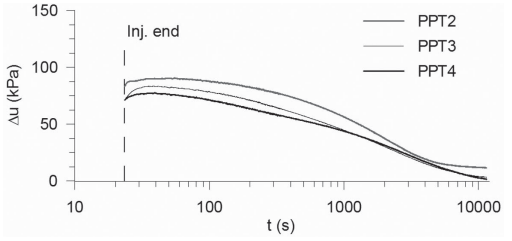

Figure 8. Excess pore water pressure measured after injection.

3 NUMERICAL SIMULATION

A numerical simulation of the injection test was carried out using the finite element method. The propagation of grout into the soil is a very difficult phenomenon to model, therefore a simple cavity expansion is introduced here to model the injection process. The study aims to asses whether it is possible to use a simple model to reproduce the effects induced by grout injections in terms of displacements, stress state and pore water pressure changes.

The axisymmetric model used for the numerical investigation of the injection test is shown in Figure 9. The mesh has a radius of 425 mm and a height of 360 mm reproducing the size of the tub used in the experiments. The initial radius of the injection cavity was taken to be equal to the radius of the injection tube (6 mm). The injection point is located at the centre of the axis of symmetry. Displacements at the base were fully constrained, while only vertical displacements were allowed along the left boundary. The interface between the soil and the container at the right boundary was modelled as an interface with reduced strength and stiffness parameters. Interface displacements are fully constrained at the right boundary.

The water head was located at the upper boundary and hydraulic flow was allowed through the lower boundary only. A 100 kPa confining pressure was applied to the upper boundary.

The injection body was modelled as a non-porous linear elastic material, with the same unit weight γ and Poisson's ratio ν of the soil, while the Young's modulus was chosen in order to optimise the calculation process, as preliminary analyses showed that the mechanical behaviour of the grout only affects the calculation time.

The mechanical behaviour of the soil was described by an elastic-plastic model with isotropic deviatoric hardening (*Hardening Soil*, HS, Schanz *et al*. 1999), implemented in the finite element code PLAXIS used for the analyses. The model is capable of reproducing soil non-linearity due to the occurrence of plastic strains from the beginning of the loading process. The elastic behaviour is defined by isotropic elasticity through a stress-dependent Young's modulus:

$$E' = E^{\text{ref}} \left(\frac{c' \cdot \cot \varphi' + \sigma_3'}{c' \cdot \cot \varphi' + p^{\text{ref}}} \right)^{\text{m}} \quad (1)$$

where σ'_3 is the minimum principal effective stress, c' is the cohesion, φ' is the angle of shearing resistance, p^{ref} = 100 kPa is a reference pressure; E^{ref} and m are model parameters.

The model has two yield surfaces, f_s and f_v, with independent isotropic hardening depending on deviatoric plastic strain γ^{p} and on volumetric plastic strains $\varepsilon^{\text{p}}{}_v$, respectively. Figure 10 shows the shape of the yield surfaces and schematically indicates their evolution.

The deviatoric hardening rule is related to parameter E'_{50}, while the volumetric one is controlled by parameter E'_{oed}. Both of them are given by expressions similar to Eq.(1) but, in contrast to E', they are not used within a concept of elasticity. The flow rule is associated for states lying on the surface f_v, while a non-associated flow rule is used for states on the surface f_s.

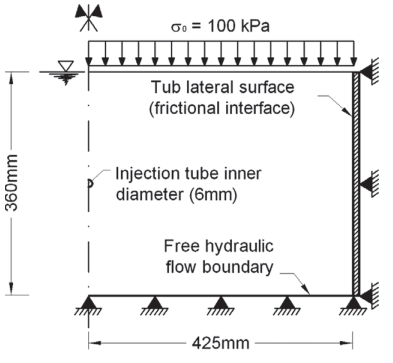

Figure 9. Finite element model for grout injection test simulation.

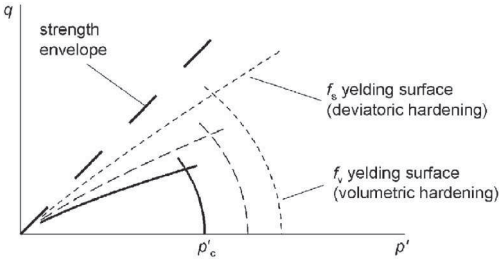

Figure 10. Yied surfaces of the Hardening Soil model and their evolution.

A feature of HS model is that under monotonic loading it can account for non-linear stress-strain behaviour, and for the occurrence of irreversible strains from the beginning of the loading process; this implies that for undrained conditions an increase of deviatoric stress q produces excess pore water pressure.

A dilatancy cut-off was introduced defining a state of density where dilatancy ends after extensive shearing. To this aim, an initial void ratio e_{init}, and a maximum void ratio e_{max} were specified. Starting from e_{init}, volume changes result in a state of maximum void e_{max}, at which the mobilised dilatancy angle ψ is set to zero.

Soil parameters were calibrated using the results of standard drained triaxial tests (TX-CID) carried out by Silva (2005) on reconstituted samples of silica flour, normally consolidated at p'_0 = 50, 100 and 200 kPa.

Since E' represents the tangent initial Young's modulus of the stress-strain curve, it has been related to the shear modulus at small strains G_0. Specifically, E'^{ref} and m were estimated from the relationship proposed by Silva (2005):

$$\frac{G}{p_a} = 300\left(\frac{p'}{p_a}\right)^{\frac{2}{3}} \tag{2}$$

where p_a is the atmospheric pressure. The remaining model parameters were calibrated best-fitting the TX-CID tests results.

Figure 11 shows the comparison between model simulations and tests results. A fair agreement between experimental data and model prediction can be obtained using the values listed in Table 3. The value of e_{init} was obtained by averaging the values of void ratio at the beginning of the deviatoric phase in the TX-CID tests. The coefficient of earth pressure at rest K_0 was estimated from:

$$K_0 = (1-\sin\varphi')\cdot OCR^{\sin\varphi'}$$

Figure 12 shows a comparison between Eq.(2) and HS model prediction (Eq.(1)), computed using the values in Table 3. A fair agreement is obtained for p' > 100 kPa.

In order to account for the different densities of triaxial test samples (D_{R1} = 100%) and the injection test sample (D_{R2} = 90%), the strength and stiffness parameters in Table 3 were corrected according to Bolton (1986):

$$\begin{aligned} &\varphi' - \varphi'_{cv} = 3DI \\ &DI = D_R\left(10 - \ln p'_f\right) - 1 \end{aligned} \tag{3}$$

where DI is a dilatancy index empirically related to the relative density D_R and to the mean effective stress at failure p'_f. Since φ'_{cv} is a state parameter, the relationship between the peak angle of shearing resistance and the relative density is obtained from Eq.(3), assuming a constant value of φ'_{cv}:

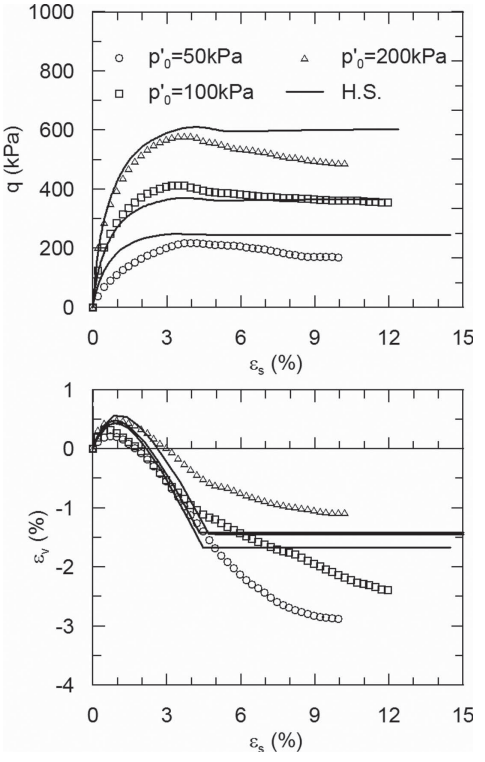

Figure 11. Comparison between TX-CID tests results and model simulation.

Table 3. Soil parameters for TX-CID tests F.E. simulation.

γ	19 kN/m^3
φ'	32.8°
c'	35 kPa
e_{init}	0.653
e_{max}	0.675
ψ	20°
ν	0.2
K_0	0.458
OCR	1
E'^{ref}	86,400 kPa
m	0.705
$E'_{50}{}^{ref}$	40,000 kPa
$E'_{oed}{}^{ref}$	22,000 kPa

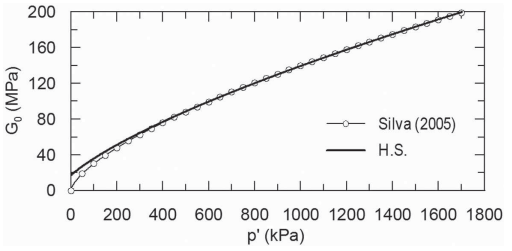

Figure 12. Comparison between Eq.(2) obtained by Silva (2005) and HS model prediction, Eq.(1).

$$\varphi'_1 - \varphi'_2 = 3(DI_1 - DI_2) \tag{4}$$

where the subscripts indicate that parameters are related to the two relative densities $D_{R,1}$ and $D_{R,2}$.

As Eq.(3) was proposed for purely frictional soils, values of φ'_1 = 38.1° and c'_1 = 0 kPa were obtained from TX-CID tests results. From Eq.(4), assuming p'_f = 237.8 kPa, it follows that φ'_2 = 37.08° and c'_2 = 0 kPa. The dilatancy angle ψ was set to zero since the initial void ratio of the injection test is higher than e_{max}. Finally, the stiffness parameters E'^{ref}, $E'_{50}{}^{ref}$ and $E'_{oed}{}^{ref}$ were scaled by the factor

$$\mu = \frac{q_{f,1}}{q_{f,2}} = \frac{M(\varphi'_1) + q_0(\varphi'_1, c'_1)}{M(\varphi'_2) + q_0(\varphi'_2, c'_2)} \tag{5}$$

where:

$$M = \frac{6\sin\varphi'}{3 - \sin\varphi'} \qquad q_0 = \frac{6c'\cos\varphi'}{3 - \sin\varphi'} \tag{6}$$

For φ'_1=32.8°, c'_1=35 kPa, φ'_2=37.08°, c'_2=0 kPa, the following values were obtained: μ = 1.353, $E'_{50}{}^{ref}$ = 63,850 kPa, $E'_{50}{}^{ref}$ = 29,560 kPa and $E'_{oed}{}^{ref}$ = 16,258 kPa.

Soil parameters used for the analyses are listed in Table 4.

As the volume of fluid drained from the sample during the test was negligible, it was assumed that the injection process resulted mainly in distortional strains, with small volume change. Hence, the analyses were carried out assuming undrained conditions.

The injection process was simulated by sequential volume expansions of the grout body. Since the experimental results showed values of compensation efficiency lower than 100% (ideal undrained conditions), the calculations were carried out applying to the grout body a volume expansion equal to the heave volume obtained at the sample surface from LVDTs readings. The analyses were carried out in terms of effective stresses, removing the hypothesis of small strains. Thus, mesh nodes coordinates were updated after each calculation step, thus allowing for the development of large strains.

Figure 13 shows the displacement profile at the upper boundary (sample surface) and the LVDT readings at the end of the injection process. The maximum heave obtained from the numerical model is sensibly larger than the experimental value and major displacements are developed near the injection body. This may be due to the vertical fracture which developed up to the top of the sample and may have spread the heave profile. In addition, a zone close around the injection body was observed to occur, where the distortional strains induced by volume expansion were very high (ε_s > 100%). Outside this zone, numerical model prediction and experimental data are in a closer agreement.

Similar features can be observed from the excess pore water pressure and stress variations profiles obtained at the injection point level, as shown in

Table 4. Hardening soil parameters for F.E. simulation of the injection test.

γ	19 kN/m^3
φ'	37.08°
c'	0 kPa
ψ	0°
ν	0.2
K_0	0.397
OCR	1
E'^{ref}	63,850 kPa
m	0.705
$E'_{50}{}^{ref}$	29,560 kPa
$E'_{oed}{}^{ref}$	16,258 kPa

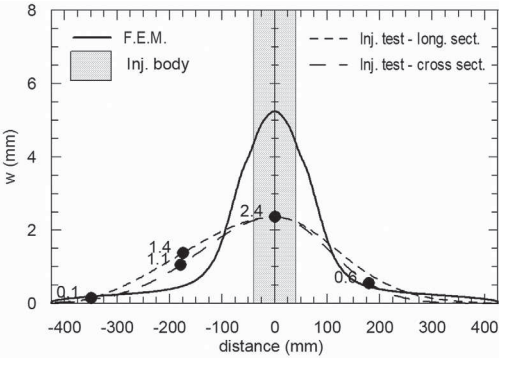

Figure 13. Surface displacements at the end of the injection.

Figure 14 and Figure 15. Within the zone of large strains, the numerical solution is not plotted since it is not accurate due to highly irregular trends. The computed excess pore water pressure and stress variations are larger than the experimental data

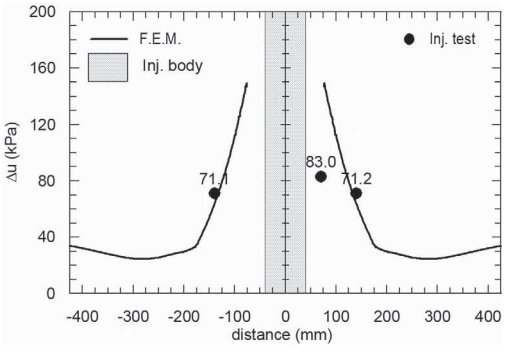

Figure 14. Excess pore pressure profile at the injection tube level, at the end of the injection.

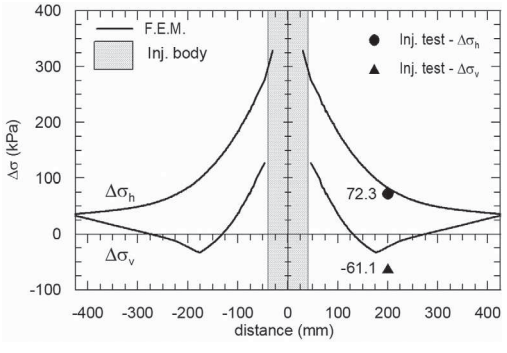

Figure 15. Stresses variation profile at the injection tube level.

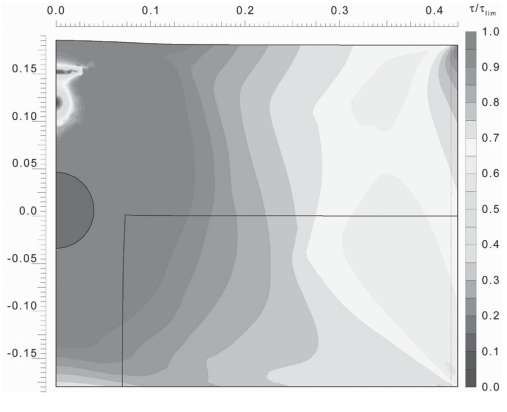

Figure 16. Mobilized shear strength contours at the end of the injection.

within a distance of about three times the injection body radius, with high gradients in the area closer to the injection body. However, a good prediction can be still obtained at greater distances.

Figure 16 shows the τ/τ_{lim} contours at the injection end. The grout expansion caused the complete mobilization of the shear stress in a large area around the injection body. The numerical results clearly show that the injection process involves the attainment of soil strength, with the development of large plastic strains.

4 CONCLUSION

The main features of grout injection in silty soil were investigated performing a laboratory injection test in a large reconstituted sample of silica flour. The experimental results show that, differently from what was observed in sandy soils, pressure filtration is negligible during the injection process, so that it does not affect grout propagation into the soil. On the other hand, it was confirmed that grout tends to develop into the soil parallel to the major principal stress.

The injection resulted in a low compensation efficiency (ξ = 26%). In addiction, data showed that the efficiency reduces with time for a normally consolidated sample, but less dramatically than what was found for clayey soils.

The injection process in silty soil was studied through a finite element analysis, simulating a cavity expansion. Specifically, the injection process was simulated by applying volume expansions to the grout body equal to the heave volume measured during the test at the top of the sample. In the analyses, the development of large strains was accounted for updating the mesh nodes coordinates after each calculation stage. The numerical results showed that the injection process induces large distortional strains in a zone around the injection body where the soil strength is fully mobilized and where displacements, excess pore water pressure and stress variations were sensibly higher than those measured. However, a satisfactory agreement with the experimental data can be achieved outside this zone, which extends about three times the radius of the injected body.

Even if the complex soil-grout interaction mechanism was not simulated, the results suggest that the effects of grout injections can be studied with simple models in term of stress changes and excess pore water pressure induced into the soil.

Although this study identifies some aspects of grout injections in silty soils, the interpretation of the test is limited by the scale of the laboratory tests. Further investigations are necessary to examine the applicability of the findings to the field scale conditions.

REFERENCES

Au, S.K.A. 2001. Fundamental Study Of Compensation Grouting In Clay. Ph.D. Thesis, University Of Cambridge. Cambridge, UK.

Au, S.K.A., Bolton, M.D. & Soga, K. 2002. Effect Of Multiple Injection On Long Term Compensation Grouting—Laboratory And Numerical Studies. *Proc. Geotechnical Aspects Of Underground Construction in Soft Ground*: 657–662. Lyon. Spécifique.

Au, S.K.A., Soga, K., Jafari, M.R., Bolton, M.D. & Komiya, K. 2003. Factors Affecting Long-Term Efficiency of Compensation Grouting In Clays. *ASCE, Journal Of Geotechnical And Geoenvironmental Engineering* 129(3): 254–262.

Au, W. 2009. An Experimental Study of Compensation Grouting in Silt, M.Phil. Thesis, University of Cambridge. Cambridge, UK.

Bezuijen, A., Sanders, M.P.M., Hamer, D.A. & Van Tol, A.F. 2007. Laboratory Tests on Compensation Grouting, The Influence Of Grout Bleeding. *Proc. 33rd Ita-Aites World Tunnel Congress*, *Prague.* Rotterdam: Balkema.

Bolton, M.D. 1986. The Strength and Dilatancy of Sand. *Géotechnique* 36(1): 65–78.

Eisa, K. 2008. Compensation Grouting In Sand. Ph.D. Thesis, University of Cambridge. Cambridge, UK.

Jaworski, G.W., Seed, H.B. & Duncan, J.M. 1981. Laboratory Study of Hydraulic Fracturing. *Asce, Journal Of Geotechnical And Geoenvironmental Engineering* 107(6): 713–732.

Mair, R.J. & Hight D.W. 1994. Compensation Grouting. *World Tunnelling:* 361–367.

Masini, L. 2010. Studio sperimentale della tecnica delle iniezioni di compensazione in terreni sabbiosi e limosi. Ph.D. Thesis, "Sapienza", University of Rome. Rome, Italy.

McKinley, J.D. 1993. Grouted Ground Anchors and the Soil Mechanics Aspects of Cement Grouting. Ph.D. Thesis, University Of Cambridge. Cambridge, UK.

McKinley, J.D. & Bolton, M.D. 1999. A Geotechnical Description of Fresh Cement Grout, Filtration and Consolidation Behaviour. *Magazine of Concrete Research* 51(5): 295–307.

Mhach, H.K. 1991. An Experimental Study of Hydraulic Fracture and Erosion. Ph.D. Thesis, City University. London, UK.

Mori, A. & Tamura, M. 1987. Hydrofracturing Pressure of Cohesive Soil. *Soils and Foundations* 27(1): 14–22.

Murdoch, L.C. 1993. Hydraulic Fracturing Of Soil During Laboratory Experiments—Part 1–3. *Géotechnique* 43(2): 255–287.

Sanders, M.P.M. 2007. Hydraulic Fracture Grouting, Laboratory Tests in Sand. M.Sc. Thesis, Delft University of Technology. Delft, the Netherlands.

Schanz, T., Vermeer, P. & Bonnier, P. 1999. Formulation and Verification of the Hardening-Soil Model. *Proc. Plaxis Symposium Beyond 2000 in Computational Geotechnics:* 281–296. Amsterdam, the Netherlands.

Silva, M.F. 2005. Numerical and Physical Models of Rate Effects in Soil Penetration. M.Sc. Thesis, University Of Cambridge. Cambridge, UK.

Yanagisawa, E. & Ali, K. 1994. Two Dimensional Study of Hydraulic Fracturing Criteria in Cohesive Soils. *Soils And Foundation* 34(1): 1–9.